Research Square

Preprints are preliminary reports that have not undergone peer review.
They should not be considered conclusive, used to inform clinical practice,
or referenced by the media as validated information.

Addressing the Regenerative Gap in Snakebite Care: UCMSC Conditioned Medium Improves Skeletal Muscle Regeneration and Attenuates Fibrosis After Bitis arietans Envenomation

Andrew Parnell
Micregen Ltd
Daniel Feist
Micregen Ltd
Mustafa Al-Asady
University of Reading
Jarred Williams
University of Reading
Atiyeh Asadpour
University of Reading
Darius Widera
University of Reading
Sakthi Vaiyapuri
University of Reading
Robert Mitchell
robertmitchell@micregen.com
Micregen Ltd
Ketan Patel
University of Reading

Research Article

Keywords: UCMSC, Stem Cells, Secretome, Conditioned Media, Muscle Regeneration, Fibrosis, Myoblast, Inflammation, NF-κB

Posted Date: November 18th, 2026

DOI: https://doi.org/10.21203/rs.3.rs-11193242/v1

License: This work is licensed under a Creative Commons Attribution 4.0 International License.
Read Full License

Additional Declarations: Competing interest reported. AP, DF, RM & KP are current or past employees of the project funder, Micregen Ltd.

Addressing the Regenerative Gap in Snakebite Care: UCMSC Conditioned Medium Improves Skeletal Muscle Regeneration and Attenuates Fibrosis After *Bitis arietans* Envenomation

Authors

Andrew Parnell[1,2]; Daniel Feist[1]; Mustafa Al-Asady[2,4]; Jarred Williams[3]; Atiyeh Asadpour[2]; Darius Widera[3]; Sakthi Vaiyapuri[3]; Robert Mitchell[1*]; Ketan Patel[1,2]

1. Micregen Ltd, The Gateway, 1 Collegiate Square, Thames Valley Science Park, Reading, RG2 9LH, United Kingdom
2. School of Biological Sciences, University of Reading, Reading, RG6 6UB, United Kingdom
3. School of Pharmacy, University of Reading, Reading, RG6 6UB, United Kingdom
4. Scientific Research Commission, Baghdad 10070, Iraq

Keywords: UCMSC, Stem Cells, Secretome, Conditioned Media, Muscle Regeneration, Fibrosis, Myoblast, Inflammation, NF-κB

* Corresponding author, Robert Mitchell PhD; Micregen, The Gateway, 1 Collegiate Square, Thames Valley Science Park, Reading, RG2 9LH, United Kingdom; robertmitchell@micregen.com

Abstract

Background

Snakebite envenomation is a WHO-recognized neglected tropical disease affecting an estimated 1.8–2.7 million people annually, with sub-Saharan Africa alone accounting for approximately 420,000 bites requiring treatment each year. Envenomation by *Bitis arietans* (Puff Adder) frequently causes severe local myotoxicity and coagulopathy, with survivors

commonly experiencing prolonged musculoskeletal disability even where antivenom is administered successfully. Current management relies on antivenom, which limits further tissue injury. However, antivenom does not address the deregulation of the muscle regeneration process caused by snake venom, which often results in long-term sequelae for victims. Umbilical cord-derived mesenchymal stem cells secrete a rich paracrine cargo of growth factors, cytokines, and extracellular vesicles that can drive myogenesis, angiogenesis, and immunomodulation in diverse injury contexts, positioning UCMSC conditioned medium as a promising cell-free regenerative candidate.

Methods

The regenerative and anti-inflammatory effects of umbilical cord-derived mesenchymal stem cell conditioned medium were assessed using in vitro and in vivo models. Human myoblast proliferation, migration, metabolic activity, and differentiation were evaluated following exposure to conditioned medium. Anti-inflammatory activity was measured using lipopolysaccharide-stimulated whole human blood and a nuclear factor kappa B reporter assay following tumour necrosis factor alpha stimulation. Interactions with venom enzymes were investigated using biochemical activity assays. A murine model of *Bitis arietans* venom-induced muscle injury was used to evaluate tissue regeneration (fibre size and quality), fibrosis, and haemorrhage. Data were analysed using appropriate statistical tests to determine significance.

Results

Extracellular vesicles derived from conditioned medium targeted human myoblasts, increasing proliferation and metabolic activity while reducing myotube fusion. Conditioned medium suppressed tumour necrosis factor alpha release and reduced nuclear factor kappa

B activation, indicating anti-inflammatory activity. It selectively inhibited venom metalloproteinase activity at low venom concentrations, did not affect phospholipase A2 activity, and increased serine protease activity. In vivo, UCMSC CM treatment increased the cross-sectional area of regenerating muscle fibres, restored dystrophin localisation, reduced fibrosis, and decreased early intramuscular haemorrhage.

Conclusions

We show that umbilical cord-derived mesenchymal stem cell conditioned medium promotes skeletal muscle regeneration and, for the first time, that it modulates key pathological features of *Bitis arietans* envenomation. Its combined regenerative, anti-inflammatory, and enzyme-modulating effects support its potential as an adjunct therapy to improve functional recovery following snakebite.

Introduction

Skeletal muscle is the largest tissue in the human body, making up about 30% to 40% of a person's body weight [1]. As well as enabling locomotion and movement, it acts as a storage depot of carbohydrates and amino acids, generates heat to maintain body temperature and maintains posture [1]. The functional cellular unit of skeletal muscle is the myofibre, which is a long cylindrical shaped cells often composed of many hundreds, if not thousands of post-mitotic nuclei.

Skeletal muscle possesses a remarkable intrinsic capacity for regeneration. A muscle can regenerate following total destruction of myofibres in a matter of weeks in rodent model systems [2]. This impressive feat is achieved through the orchestrated action of several cells, including the resident stem cells of skeletal muscle called satellite cells, as well as a large number of other players that include immune cells and fibro-adipogenic progenitors (FAPs),

which enable the clearance of necrotic matter, promote myogenesis and tissue remodelling [3]. Under conditions of persistent or repeated injury, this orderly progression can be disrupted, resulting in impaired regeneration and replacement of muscle tissue with fibrotic and adipose tissue rather than functional myofibres, a phenomenon well documented in chronic neuromuscular disease [4] and in the context of this study, after snakebite envenomation [5].

Snakebite envenomation was formally recognised by the World Health Organization (WHO) as a category A neglected tropical disease in 2017, reflecting its substantial and long-underappreciated global health burden [6]. An estimated 1.8 to 2.7 million envenomations and up to 81,000 to 138,000 deaths occur worldwide each year [7], with sub-Saharan Africa accounting for roughly 270,000 to 300,000 cases and 32,000 to 38,000 deaths annually [8, 9]. Beyond mortality, snakebite survivors frequently experience long-term physical disability, with musculoskeletal impairment representing the most common chronic sequela, driven largely by local tissue destruction at the bite site that current treatments are not designed to reverse [10, 11]. Viperid envenomation, including those caused by Puff Adder (*Bitis arietans*), is particularly associated with profound local tissue damage, haemorrhage, and coagulopathy, in contrast to the predominantly neurotoxic presentation of elapid bites [12, 13]. *B. arietans* is one of the most medically significant snakes across sub-Saharan Africa, being responsible for more envenomations than all other snake species in the continent combined. *B. arietans* venom (BaV) is known to cause extensive skeletal muscle necrosis, oedema, and haemorrhage at the site of injection, with clinical case series consistently describing local myotoxic and hemotoxic effects following envenomation [14].

The pathophysiology of BaV-induced tissue damage is driven substantially by a cocktail of enzymatically active toxins, most notably snake venom metalloproteinases (SVMPs), which degrade extracellular matrix and basement membrane components and disrupt microvascular integrity and snake venom serine proteases (SVSPs), which exhibit thrombin-like activity and contribute to venom-induced consumption coagulopathy. Additionally, phospholipase A_2 (PLA_2) enzymes, which directly damage myofibre membranes and C-type lectin-like proteins (CLPs/CTLs), which modulate blood clotting and platelet activation, are also present in substantial abundance [15].

Current clinical management of *B. arietans* envenomation centres on antivenom administration. While this intervention can be effective at neutralising venom components when administered promptly, they are fundamentally limited in two respects: their efficacy is highly dependent on the time elapsed between bite and treatment, and, even when successful, they do not actively promote the regeneration of muscle tissue already damaged.

Mesenchymal stem cells (MSCs) have been extensively investigated for their regenerative potential across a wide range of tissue injury models [16]. While early work focused on their capacity to differentiate directly into resident cell types, substantial evidence has since demonstrated that MSCs exert most of their therapeutic benefit through paracrine signalling, via secreted growth factors, cytokines, and extracellular vesicles (EVs) collectively referred to as the secretome, rather than through cell engraftment and differentiation [17-19]. This shift in understanding has driven considerable interest in MSC conditioned medium (CM) and MSC-derived EVs as cell-free, more readily standardised and scalable alternatives to whole-cell therapy, with the added advantage of avoiding risks associated with live cell transplantation, such as uncontrolled proliferation or immune rejection [20].

Umbilical cord-derived MSCs (UCMSCs) are an increasingly favoured source for such secretome-based approaches, owing to their non-invasive, ethically straightforward collection, high proliferative capacity, low immunogenicity, and stable genetic background relative to bone marrow or adipose-derived MSCs [21-23]. In this study, we hypothesised that the regenerative and immunomodulatory paracrine activity of UCMSC CM's extends to BaV-induced skeletal muscle injury, promoting muscle regeneration through a combination of direct effects on myogenic cells, modulation of the injury-associated inflammatory response, and interaction with the enzymatic components of venom itself. To test this, we combined in vitro assays of myoblast proliferation, migration, differentiation, and inflammatory signalling with direct biochemical characterisation of UCMSC CM's effects on venom enzyme activity and assessed the translational relevance of these findings in a murine model of BaV-induced acute skeletal muscle injury, evaluating myofibre regeneration, fibrosis, and haemorrhage at two post-injury time points. Our findings position UCMSC CM as a candidate regenerative and anti-fibrotic adjunct therapy, distinct in mechanism from existing venom-neutralising treatments, for a condition where the current standard of care leaves a substantial and unaddressed burden of long-term tissue damage.

Materials and Methods

Cell culture

Human UCMSCs (RoosterBio® RoosterVial™ hUC-20M-CC, C04020UC) were cultured in RoosterNourish™-MSC-XF media (RoosterBio®, KT-016) with 1% Penicillin-Streptomycin (Gibco™, 15140-122).

Immortal human myoblasts, AB1190 (The Institute of Myology, Paris, France), were cultured in Skeletal Muscle Culture Media (PromoCell®, C-23060), with 1% Penicillin-Streptomycin (Gibco™, 15140-122).

UCMSC conditioned media generation

Confluent flasks of UCMSCs were washed thrice in Earles Balanced Salt Solution (EBSS), prior to generating conditioned media (CM) for 48 hours in fresh EBSS. Following incubation, CM and cells were separated by centrifugation for 10 minutes at 300 RCF. CM was further processed, first with a 2,000 RCF centrifugation for 20 minutes, and second with 0.22 µm filtration. CM was stored at 2- 8 °C for up to 1 month. CM was generated from UCMSC between passages 5 and 7.

UCMSC-derived EV uptake assay

AB1190 cells were seeded at low density (1,000 cells) in black-walled, clear-bottom 96-well plates, and allowed to adhere overnight at 37°C with 5% CO_2. UCMSC-derived EVs, isolated from UCMSC CM by ultrafiltration using 100 kDa centrifugal filters (Merck Amicon™ Ultra-15, 10188431), were labelled with PKH67 (Sigma, MIDI67), washed in 1% BSA in EBSS, and resuspended in EBSS. In parallel, an EV-free vehicle control was prepared by processing CM vehicle through the same ultrafiltration and PKH67-labelling process. Following attachment, AB1190 cells were stained with CellTracker™ Deep Red (DR) (Invitrogen™, C34565) for 30 minutes in EV-free culture media, washed thrice prior to incubation for 24-hours if PKH67-labelled EVs or PKH67-vehicle at a total EV number equivalent to a 10% v/v UCMSC CM treatment in EV-free culture media. Following incubation, cells were washed thrice and fixed in 4% PFA and counterstained with DAPI. EV uptake was imaged and quantified using Revvity Operetta CLS high-content imaging system, with CellTracker™ DR signal defining the cell area,

158 DAPI defining nuclei, and PKH67 fluorescence intensity withing cytoplasmic region (cell area
159 minus nucleus) taken as a measure of EV internalisation.

160 Cellular proliferation assay

161 AB1190 cells were seeded at low density (500 cells) in black-walled, clear-bottom 96-well
162 plates, and allowed to adhere for 5 hours at 37°C with 5% CO_2. Following adherence, the
163 culture media was aspirated and replaced with treatments (10% v/v UCMSC CM or vehicle in
164 reduced (25% of normal) skeletal muscle culture media supplement) and incubated for 96
165 hours at 37°C with 5% CO_2. Following incubation, test media were removed, and cells were
166 washed once with PBS prior to freezing dry at -80°C. On the day of seeding, AB1190 cells were
167 also seeded in a known cell number-dilution series. Following a 5-hour attachment phase, the
168 plate was washed and frozen dry. Analysis of cell proliferation was performed using CyQuant®
169 cellular proliferation kit (Thermo Scientific™, C7026), following the manufacturer's
170 instructions.

171 Cell migration assay

172 AB1190 cells were seeded at a density of 2,000 cells per well of a 24-well plate and allowed
173 to adhere overnight at 37°C with 5% CO_2. Following adherence, culture media was aspirated
174 and replaced with treatments (10% v/v UCMSC CM or vehicle in skeletal muscle culture media
175 supplement). Time-lapse images were captured every 10 minutes over a 23-hour period using
176 a Nikon Eclipse Ti-E microscope with NIS Elements software, and movies were created. Cell
177 migration (speed) was measured using CellTracker Software [24]

178 Assessment of mitochondrial and lysosomal content

AB1190 human myocytes were seeded in black-walled, clear-bottom 96-well plates at 1,000 cells per well and allowed to adhere overnight at 37°C, 5% CO_2 in standard culture medium. After attachment, medium was replaced with fresh medium containing 10% v/v UCMSC CM or vehicle, and cells were incubated for a further 24 hours. Treatment medium was then removed, and cells were washed thrice with EBSS prior to addition of vital dye-cocktail (Hoechst 34580 (Invitrogen™, H21486), Calcein AM Green (Invitrogen™, C34852) and either MitoTracker™ Deep Red (Invitrogen™, M22426) or LysoTracker™ Red DND-99 (Invitrogen™, L7528) in EBSS) for a 30-minute incubation at 37°C, 5% CO_2. Cells were visualised and imaged immediately on a Revvity Operetta CLS High-Content Analysis System. MitoTracker™ Deep Red or LysoTracker™ Red intensity within the Calcein AM Green–positive cytoplasmic region was used as a measure of mitochondrial mass and lysosomal content, respectively.

AB1190 differentiation assay

AB1190 myocytes were seeded into 24-well tissue culture plates and grown to 80–90% confluence. Culture medium was then replaced with differentiation medium (Skeletal Muscle Cell Growth Medium; PromoCell®, C-23260) supplemented with 5% horse serum (Gibco™, 26050-070) and 1% penicillin–streptomycin (Gibco™, 15140-122), and cells were cultured for 4 days at 37°C, 5% CO_2 with 10% (v/v) UCMSC CM or vehicle added at the start of differentiation.

After 4 days, cells were fixed with 4% PFA for 15 minutes at room temperature and washed three times with PBS. Cells were permeabilised for 15 minutes (20 mM HEPES, 3 mM $MgCl_2$, 50 mM NaCl, 300 mM sucrose, 0.5% Triton X-100, 0.05% NaN_3), rinsed three times with PBS, then blocked for 1 hour in 5% foetal bovine serum, 0.05% Triton X-100 in PBS. A pan-myosin primary antibody (A4.1025, mouse monoclonal, Developmental Studies Hybridoma Bank)

diluted 1:200 in blocking buffer was applied for 2 hours at room temperature, followed by three 5-minute washes in blocking buffer. An anti-mouse IgG fluorescent secondary antibody (Invitrogen™, A11029; 1:200 in blocking buffer) was then incubated for 1 hour at room temperature in the dark, washed twice for 5 minutes in blocking buffer and once in PBS. Nuclei were counterstained with DAPI (300 nM in PBS, 10 minutes), followed by three PBS washes.

Fluorescent images were acquired using a Keyence BZ-X810 microscope, and fusion index was quantified with the open-source Myotube Analyzer software [25].

Whole Blood inflammation assay

Whole human blood was collected from consenting volunteers (Biological Sciences' Research Ethics Committee at the University of Reading, project title: "Effects of Stem Cell Secretomes on Inflammation", reference code: SBS22-23 41, approved on: 25 January 2023) using a heparin-coated vacutainer®.

200 µL of blood was added to a 24 well plate together with 600 µL of RPMI 1640 media (PAN Biotech, P04-18047) and 100 µL UCMSC CM concentrations before being incubated for 1 hour. Following incubation, 100 µL of 10 ng/mL *E. coli* LPS/RPMI media was added to each 'stressed' well with only RPMI media to control wells and the cells incubated for a further 5 hours at 37°C, 5% CO_2. Following incubation, the suspension was centrifuged at 2,000 RCF for 20 min and the supernatant collected and frozen at -80°C.

TNFα concentration was measured via ELISA (R&D Systems DY210) following manufacturer's instructions. Briefly, a 96 well plate was coated overnight at room temperature with 100 µL of the Capture Antibody before blocking with BSA for 1 hour and addition of test sample or standards for a 2-hour incubation at room temperature. 100 µL

Detection Antibody was added for a 2-hour incubation before protein concentration was detected at 450 nm absorbance following incubation for 20 min with Streptavidin-HRP.

U251 NF-κB-reporter inflammation

U251 cells (ECACC) transduced with a lentiviral pGreenFire™-NF-κB-GFP-Luciferase reporter construct [26] were cultured in high-glucose DMEM (Sigma Aldrich) supplemented with 1% L-glutamine (200 mM; Sigma Aldrich), 10% FBS (Sigma Aldrich) and puromycin (1 µg/ml) at 37°C and 5% CO_2. Cells were seeded in 96-well plates at 1×10^4 cells/well and incubated for 24 hours to allow attachment. They were then pretreated for 24 hours with 2% UCMSC CM, followed by 4 hours of serum starvation in medium containing 0.01% BSA at 37°C and 5% CO_2, with 2% (v/v) UCMSC CM added to the appropriate wells. Cells were subsequently returned to complete serum-containing medium and treated with 2% UCMSC CM and TNFα (10 ng/mL) for 24 hours. After incubation, culture medium was replaced with phenol red-free DMEM (Sigma-Aldrich, UK), and Bright-Glo® substrate (Promega, UK) was added directly to the wells according to the manufacturer's protocol. Luminescence was measured using a SpectraMax i3x microplate reader (Molecular Devices, UK), with signal intensity used to quantify NF-κB reporter activity.

Snake venom metalloproteinase assay

SVMP activity was assessed by monitoring cleavage of the fluorescent substrate DQ™ Gelatin. *Bitis arietans* venom (BaV) was diluted in UCMSC CM or vehicle to final concentrations of 4, 8, 16, or 32 µg/mL. 2 µL of DQ™ Gelatin (1 mg/mL; Invitrogen™, D12054) were added to black-walled, clear-bottom 96-well plates, followed by 98 µL of BaV/conditioned media mixtures. Fluorescence (ex 485 nm, em 520 nm) was recorded immediately and then every 10 minutes

246 for 90 minutes using a FLUOstar Omega plate reader (BMG LABTECH). Wells containing only
247 vehicle or UCMSC CM were used to normalize baseline fluorescence.

248 Snake venom serine protease assay

249 SVSP activity was measured using the fluorescent substrate Nα-Benzoyl-L-Arginine-7-Amido-
250 4-methylcoumarin hydrochloride (BAAM-C). BaV was diluted in UCMSC CM or vehicle to final
251 concentrations of 4, 8, 16, or 32 µg/mL. 2 µL of BAAM-C (2 nM/mL; Sigma-Aldrich, B7260)
252 were dispensed into black-walled, clear-bottom 96-well plates, followed by 98 µL of
253 BaV/conditioned media mixtures. Fluorescence (ex 355 nm, em 460 nm) was measured
254 immediately and then every 10 minutes for 90 minutes on a FLUOstar Omega plate reader.
255 Wells containing only vehicle or UCMSC CM served to normalize baseline fluorescence.

256 Snake venom phospholipase A_2 assay

257 PLA_2 activity was quantified using the chromogenic substrate NOB. BaV was diluted in UCMSC
258 CM or vehicle to final concentrations of 8, 16, 32, or 64 µg/mL. In clear 96-well plates, 20 µL
259 NOB (3.1 mg/mL in acetonitrile; Abcam, ab141769) were mixed with 20 µL ddH_2O and 200 µL
260 PLA_2 reaction buffer (10 mM Tris-HCl, 10 mM $CaCl_2$, 100 mM NaCl), followed by addition of 20
261 µL BaV/conditioned media mixtures. Absorbance at 425 nm was recorded immediately and
262 then every 10 minutes for 120 minutes using a FLUOstar Omega plate reader. Wells containing
263 only vehicle or UCMSC CM were used to normalize baseline absorbance.

264 Home Office license and ethics statement for animal research

265 All animal procedures were conducted in accordance with the Animals (Scientific Procedures)
266 Act 1986 (ASPA) and the EU Directive 2010/63/EU, under UK Home Office project license
267 (project title: “Optimising skeletal muscle structure and function to withstand the challenges

of damage and ageing", licence number: PP8746932, approved on 06 September 2022) and personal licenses held by named individuals, at the University of Reading (establishment license: XF75DBBCB). The study was approved by the University of Reading's Animal Welfare and Ethics Review Board (AWERB) prior to commencement. Reporting follows the ARRIVE 2.0 guidelines. Male C57BL/6 mice were obtained from Charles River Laboratories and allowed a minimum acclimatisation period of 4 days prior to experimentation. Animals were housed in groups of 3 to 5 mice per cage under specific pathogen-free conditions with a 12:12 hour light:dark cycle, temperature of 21±2°C, humidity of 55±10%, and environmental enrichment (for example nesting material, tunnels, chew blocks and scatter feeding), with ad libitum access to food and water.

Muscle regeneration model

C57BL/6 mice were divided into treatment groups (n=5 naïve, n=8 day 5 BaV + vehicle, n=8 day 5 BaV + UCMSC CM, n=8 day 15 BaV + vehicle, n=8 day 15 BaV + UCMSC CM) Muscle damage was induced by intramuscular (IM) injection of *B. arietans* venom (BaV; 0.8 µg/g body weight in 30 µL sterile saline; VenomTech Ltd) into the right tibialis anterior (TA) under general anaesthesia (induction: 5% isoflurane in 2 L/min O_2; maintenance: 2% isoflurane in 2 L/min O_2).

UCMSC CM or vehicle was administered as a 5 µL/g body weight intraperitoneal (IP) bolus 1 hour prior to BaV injection (day 0), then once daily until day 4 for both day 5 and day 15 cohorts. For the day 15 cohort, additional IP doses were given on days 5, 8, 11, and 14. Animals were euthanized by CO_2 asphyxiation followed by cervical dislocation, in accordance with Schedule One of the Animals (Scientific Procedures) Act 1986.

Sample size justification

The primary outcome for sample size determination was the mean cross-sectional area (CSA) of $eMHC^+$ regenerating myofibres at day 5 post-BaV injury, comparing BaV + Vehicle and BaV + UCMSC CM. Based off previous work with BaV [27] and MSC-derived CM treatment of other venom-induced muscle damage models [28], power calculations using G*Power Software (d=2, α=0.05, power = 0.8) estimated the required sample size as n=6 animals per group. To allow for biological variability and potential data loss, 6-8 mice per group were used in this study.

Randomisation and blinding

Animals were allocated to treatment groups by an impartial technician using block randomisation stratified by cage. The study was conducted unblinded until endpoint analysis of muscle sections.

Inclusion/exclusion criteria

Pre-specified exclusion criteria included: failed or misplaced intramuscular venom injection (confirmed by absence of visible local injury), missed or incomplete UCMSC CM/vehicle IP administration, technical failure during tissue processing (e.g., section damage precluding quantification), and any animal meeting humane endpoint criteria requiring early euthanasia (see below). No animals were excluded due to failure to inject, and no animals were excluded due to early euthanasia. Up to 4 animals were excluded due to technical failure during tissue processing.

Animal Welfare Monitoring and Human Endpoints

Following BaV injection, animals were monitored continuously for 30 minutes and at least twice daily for signs of pain, distress, or excessive local tissue damage. Pre-defined humane

endpoints requiring early euthanasia included greater than 10% body weight loss, severe lameness, and signs of systemic toxicity. Animals received 0.1 mg/kg SC buprenorphine at time of BaV IM injection for post-procedural analgesia.

Tissue harvest, processing and staining

Following euthanasia, right tibialis anterior (TA) muscles were dissected, weighed, snap-frozen in liquid nitrogen–cooled isopentane, and stored at −80°C until processing. Muscles were embedded in OCT (Cell Path Ltd, KMA-0100-00A), and 15 µm transverse sections were cut from the mid-belly using a cryostat and stored at −80°C.

For haematoxylin and eosin (H&E) staining, sections were equilibrated to room temperature, rinsed in PBS to remove excess OCT, stained with Harris haematoxylin (Thermo Scientific™, 12627926), differentiated in acid alcohol, blued under running tap water, and counterstained with Eosin Y (Sigma Aldrich, 318906-500mL). Sections were then dehydrated through graded ethanol, cleared in xylene, and mounted with DPX (Fisher Scientific, D/5330/05).

For picrosirius red staining, sections were brought to room temperature, incubated in pre-warmed Bouin's solution (Sigma Aldrich, SLCP7185), washed in distilled water, and stained with picrosirius red (Abcam, ab246832) before rinsing in 0.5% glacial acetic acid. Sections were subsequently dehydrated, cleared in xylene, and mounted with DPX. Fibrosis was quantified in ImageJ using threshold-based analysis, expressing picrosirius red–positive area in damaged regions (200 μm^2) relative to a reference area from undamaged muscle (500 μm^2).

For immunohistochemistry, sections were equilibrated to room temperature, circumscribed with a hydrophobic barrier, and washed in PBS. Sections were permeabilized (20 mM HEPES, 3 mM $MgCl_2$, 50 mM NaCl, 300 mM sucrose, 0.5% Triton X-100, 0.05% NaN_3) and blocked (5%

foetal bovine serum, 0.05% Triton X-100 in PBS) before incubation with primary antibodies diluted in blocking buffer (Table 1) overnight at 4°C. After three washes in blocking buffer, fluorophore-conjugated secondary antibodies (Table 2) were applied for 1 hour at room temperature in the dark. Sections were washed, then mounted in DAKO fluorescent mounting medium containing 2.5 µg/mL DAPI.

Brightfield images of H&E–stained sections were acquired at 40× using a Hamamatsu NanoZoomer-SQ digital slide scanner, and images were stitched for analysis. Picrosirius red and immunofluorescence images were obtained using a Keyence BZ-X810 fluorescence microscope: sections were located at 2×, then imaged at 10× with automated focusing and appropriate filter sets (brightfield, DAPI/blue, 488/green, 546/594/red). Exposure times were optimized for each stain and kept constant within experimental sets, and images were stitched prior to quantitative analysis.

Table 1 Primary antibodies used for immunohistochemical analysis of muscle.

Target	Host	Dilution	Catalogue information	Lot Number
Dystrophin	Rabbit IgG	1 in 400	Abcam, ab15277	GR3417779-1
Fibrinogen	Rabbit IgG-FITC	1 in 200	Dako, F0111	41693429
Laminin	Rabbit IgG	1 in 1000	Invitrogen, PA1-16730	ZH4441303
eMHC	Mouse IgG	1 in 200	Santa Cruz, sc-53091	H1518
PDGFRα	Rabbit IgG	1 in 500	Abcam, ab203491	1076010-16

Table 2 Secondary antibodies used for immunohistochemical analysis of muscle.

Target	Host	Dilution	Catalogue information	Lot Number
Anti-Rabbit IgG	Goat IgG – Alexa 488	1 in 200	Invitrogen, A11034	2018207
Anti-Rabbit IgG	Goat IgG – Alexa 594	1 in 200	Invitrogen, A11037	2005936
Anti-Mouse IgG	Goat IgG – Alexa 546	1 in 200	Invitrogen, A11003	1107499

Muscle analysis

Cross-sectional areas for eMHC and CLN-positive myofibres were automatically measured using CellPose v4 and Image J. Firstly, positive fibres were selected from a 500 x 500 µM area of damaged tissue using CellPose v4 [29] to generate a mask. Laminin was used to determine the perimeter of myofibres. Image masks were input into ImageJ Plugin "LabelsToROIs" [30], with the number of pixels to erode set to 1.

Dystrophin sarcolemmal coverage was automatically quantified using CellPose v4 and ImageJ. Firstly, fibres were selected from a 500 x 500 µM area of damaged tissue using CellPose v4 to generate a mask. Dystrophin was used to determine the perimeter of myofibres. Image masks were input into a custom ImageJ Plugin which generates individual fibre regions of interest along the membrane. Dystrophin coverage was calculated as the percentage of the myofibre circumference containing dystrophin-positive signal.

For the remainder of the muscle stains, Picrosirius, PDGFRα and fibrinogen, analysis was conducted using Keyence BZ-X800 Analyzer software to identify positively stained areas in muscle sections.

Statistical analysis

Data are presented as mean values unless otherwise stated. Statistical analyses were performed using GraphPad Prism (version 10 or later). Two-tailed t-tests were used to compare two independent groups when no directional hypothesis was specified. One-way or two-way ANOVA was applied for comparisons involving more than two groups or more than one independent factor, respectively, with assessment of main effects and interactions. Where ANOVA indicated a significant effect, post hoc multiple-comparison tests were used as

appropriate: Tukey's test for all pairwise comparisons, Dunnett's test for multiple treatments versus a single control, and Sidak's correction for predefined subsets of comparisons. Assumptions of normality and homogeneity of variance were verified before applying parametric tests. A significance threshold of $\alpha = 0.05$ was used, and statistical significance is indicated as follows: * $p < 0.05$; ** $p < 0.01$; *** $p < 0.001$; **** $p < 0.0001$.

Results

Impact of UCMSC CM on myoblast characteristics.

We first showed that muscle cells could be direct targets of components of UCMSC CM. To that end, PKH-67-labelled EVs derived from UCMSC CM were incubated with AB1190 cells, a human myoblast line. Subsequent 3D fluorescent imaging revealed that UCMSC-derived EVs were taken up by target cells as indicated by intracellular PKH-67 signals (Figure 1A). AB1190 cells incubated with PKH-EVs had a greater level of fluorescent signal within the cytoplasmic region compared to the control, 29.8 to 1,031 RFU ($p<0.0001$) (Figure 1B).

Next, the effects of UCMSC CM on cellular characteristics of AB1190s were assessed. A cellular proliferation assay revealed that UCMSC CM significantly increased the number of AB1190 cells compared to the vehicle by 15.6% ($p<0.0001$) (Figure 1C), whereas single-cell tracking found no difference in AB1190 migration speed with UCMSC CM treatment (Figure 1D).

The status of two intracellular organelles was also assessed using vital dyes. First, the abundance of lysosomes in AB1190 was found to be statistically increased by 22.5% after a 24-hour treatment with UCMSC CM ($p=0.0042$) (Figure 1E). Similarly, the mitochondrial mass was also found to significantly increase after a 24-hour treatment with UCMSC CM, up by 12.4% ($p=0.0341$) (Figure 1F).

Finally, we examined the differentiation of AB1190 myoblasts into myotubes. Here, the degree of cell fusion was determined by indexing the number of nuclei per myotube against the undifferentiated cells. We found that UCMSC CM significantly reduced the amount of myoblast fusion over a 4-day period, from an index of 0.13 to 0.08 ($p=0.0397$).

The effect of UCMSC CM on inflammation.

To determine whether UCMSC CM could modulate an inflammatory response, whole human blood was challenged with bacterial LPS in the presence or absence of UCMSC CM, and secreted TNFα was quantified by ELISA. LPS stimulation significantly increased TNFα concentration compared to baseline unstimulated levels ($p<0.0001$), with stimulated TNFα levels normalised to 100.0%. Increasing concentrations of UCMSC CM reduced the amount of LPS-induced TNFα significantly in a dose-dependent manner (Figure 1I), from no reduction in TNFα with the lowest CM concentration 0.001x UCMSC CM at 98.3% of stressed controls, 0.01x reducing TNFα to 58.3% ($p=0.0003$), 0.1x to 27.1% ($p<0.0001$) and 1x to 12.3% ($p<0.0001$) compared to the vehicle.

Next, to determine whether this effect involved modulation of NF-κB signalling, a pathway central to a cell's response to inflammatory stimuli, U251 cells stably expressing an NF-κB-GFP-luciferase reporter were utilised (Figure 1J). Here, TNFα stimulation significantly increased NF-κB reporter activity compared to unstimulated controls, from 7.4 RLU to 78.4 RLU ($p<0.0001$). UCMSC CM treatment significantly attenuated this increase, reducing luminescence to 52.3 RLU ($p=0.0401$), indicating that UCMSC CM dampens NF-κB pathway activation downstream of an inflammatory stimulus.

UCMSC CM modification of enzyme activity.

To investigate if UCMSC CM has the ability to directly modulate the activity of enzymes found in snake venom, three fluorescent-ligand assays were utilised. In all cases, increasing concentrations of snake venom were used, and the rate of substrate metabolism was measured over time. Snake venom metalloproteinase (SVMP) activity was observed to be reduced in the presence of UCMSC CM compared to vehicle controls, reaching significance at concentrations lower than 8 µg/mL BaV (Figure 2A). After 90 minutes, the amount of fluorescence, indicative of catabolic activity, with 4 µg/mL BaV was reduced from 6.2 to 4.6 RFU ($p=0.0082$) and from 8.6 to 7.5 RFU ($p=0.0127$) at 8 µg/mL BaV. At 16 µg/mL BaV UCMSC CM non-significantly reduced SVMP activity to 10.5 RFU from 11.4 RFU, and for 32 µg/mL BaV, from 13.5 to 12.9 RFU. Furthermore, there was no inherent SVMP activity from UCMSC CM in the absence of BaV.

Next, the impact on snake venom serine protease (SVSP) activity was explored, which exhibit thrombin-like activity. UCMSC CM was found to increase the SVSP activity, which was more pronounced at the higher BaV concentrations (Figure 2B). After 90 minutes with 8 µg/mL BaV, UCMSC CM increased florescence from 0.15 to 0.35 RFU ($p=0.0034$), from 0.46 to 0.78 RFU with 16 µg/mL BaV ($p=0.0011$), and from 1.1 to 1.6 RFU with 32 µg/mL BaV ($p=0.0166$). As with SVMP activity, there was no detectable SVSP activity in UCMSC CM in the absence of BaV.

The third enzyme assessed was phospholipase A_2 (PLA_2) activity. Due to the lower levels of PLA_2 found in BaV, the range of concentrations tested was higher than MP and SP. However, there was no detectable change in PLA_2 activity with the addition of UCMSC CM, nor was there any inherent enzymatic activity from the CM (Figure 2C).

<u>UCMSC CM as a treatment for *B. arietans*-induced skeletal muscle damage.</u>

An acute BaV-induced skeletal muscle injury model was used to assess the impact of systemically administered UCMSC CM on muscle regeneration. Myofibre regeneration was first evaluated at 5 days post-injury. During the initial stages of regeneration, newly formed myofibres express embryonic myosin heavy chain (eMHC) before transitioning to adult myosin heavy chain isoforms. Thus, eMHC expression serves as a marker of actively regenerating myofibres, while fibre size provides an indication of regenerative progression (Figure 3A). Analysis of regenerating fibres showed no statistical difference in the cross-sectional area (CSA) of eMHC–positive fibres at day 5 following BaV injury. Untreated *Tibialis Anterior* (TA) muscles exhibited an average cross-sectional area of 304.8 μm^2, compared to 341.3 μm^2 in UCMSC CM-treated TAs (p=0.5886) (Figure 3C).

By day 15 post-injury, there were almost no eMHC actively regenerating myofibres. Instead, regenerated myofibres, identified as centrally nucleated fibres (CNF) were present throughout the muscle. CNF were significantly larger following UCMSC CM treatment compared to the vehicle treatment, with the average CSA measured at 1,261.0 μm^2 compared to 692.6 μm^2 (p=0.0063) (Figure 3D). CNF in both groups remained significantly smaller at day 15 than healthy myofibres in undamaged TAs, with their average CSA measuring 1,869.0 μm^2. Next, the quality of the regenerated myofibres was examined. Dystrophin, a submembrane protein essential for maintaining myofibre structural integrity, was assessed. In healthy muscle, dystrophin is uniformly distributed along the membrane; however, in damaged or poorly regenerated myofibres, its expression is often uneven or reduced (Figure 3B). As such, dystrophin localisation and abundance can be used to assess fibre quality. At day 5 post-injury, dystrophin expression was markedly reduced in the damaged regions in both conditions (Figure 3B). Quantitative assessment of the presence of dystrophin around the circumference of CNF at day 15 post-injury revealed that untreated TAs had significantly incomplete

membrane localisation in the regenerated myofibres, at 78.4% circularity, compared to an average of 99.5% circularity in healthy myofibres in undamaged TAs (p=0.0009) (Figure 3D). Following UCMSC CM treatment, dystrophin localisation around the membrane was significantly greater than the vehicle group, at 95.3% (p=0.0015), which was found to be non-significant compared to the baseline healthy myofibres (Figure 3E).

UCMSC CM reduces fibrosis in TA after BaV injury.

Haematoxylin and Eosin (H&E) histological assessment of the TAs revealed both the extent of muscle damage and regeneration at day 5 and day 15. Undamaged muscle displays a uniform mosaic of myofibres with peripherally located myonuclei, organised into bundles separated by a thin extracellular matrix. 5 days following BaV-induced injury, this architecture was largely replaced by infiltrating leukocytes, including macrophages and neutrophils, as indicated by white arrows (Figure 4A). The regenerating myofibres were also evident, characterised by their smaller size and centrally located nuclei (red arrows). By day 15, infiltration had partially resolved, and a greater number of myofibres exhibited centrally located nuclei.

The H&E analysis showed the presence of acellular deposits in muscle after BaV-induced muscle damage. This material could represent fibrotic tissue. To investigate the effect of UCMSC CM on the development of fibrosis after BA venom injection, muscle sections were stained with Picrosirius Red (PSR) (Figure 4B). At day 5 post-injury, PSR staining was widely distributed throughout the damaged regions of the muscle (white arrows), comprising 58.7% in vehicle-treated animals and 59.3% of the total muscle area in the UCMSC CM-treated group (Figure 4D). In undamaged muscle, PSR staining accounted for only 9.0% of the total muscle area. By day 15, PSR staining closely resembled that of undamaged muscle, forming around myofibres. However, the deposits were denser, consistent with fibrotic remodelling (green

arrows). Vehicle-treated animals contained fibrotic lesions covering 51.1% of the muscle area, which was significantly reduced in UCMSC CM-treated muscle to 33.6% (p=0.0012) (Figure 4D).

To explore whether UCMSC CM reduced fibrosis by modulation of fibro-adipogenic progenitors (FAPs), the level of FAP marker platelet-derived growth factor receptor alpha (PDGFRα) was examined (Figure 4C). Baseline FAP levels in undamaged TAs were 2.1% of the muscle area, which increased to 7.5% in vehicle-treated BaV-damaged muscles at day 5 (Figure 4E). At day 5, there was no statistical difference to UCMSC CM treatment, with FAP levels at 6.5%. By day 15, FAP abundance further increased to 10.9% in the vehicle group. In contrast, UCMSC CM treatment maintained FAP levels comparable to day 5, with 6.8% PDGFRα expression in the muscle, which were significantly lower than the vehicle group (p=0.0396).

Finally, BaV is known to exhibit haemorrhagic activity, which is frequently reported in the clinical setting [31]. To determine whether UCMSC CM influenced haemorrhage, staining for the blood protein fibrinogen was performed to detect intramuscular blood accumulation (Figure 5A). At day 5 post-injury, fibrinogen occupied 9.8% of the muscle area in vehicle-treated animals (Figure 5B). UCMSC CM treatment significantly reduced the abundance of fibrinogen to 6.1% (p=0.0362) at this time point. By day 15, there was no evidence of ongoing haemorrhage, with fibrinogen levels returning to baseline: 0.6% for the undamaged fibres and day 15 vehicle-treated, and 0.7% for UCMSC CM-treated groups, respectively.

Discussion

Skeletal muscle damage is often a major consequence of snake envenomation, contributing substantially to long-term morbidity through incomplete functional recovery, which leads to persistent weakness and fibrosis even in patients who receive antivenom in a timely manner.

Against this clinical backdrop, therapies that actively improve the quality and pace of skeletal muscle regeneration following snakebite envenomation and limit permanent disability remain scarce, with current interventions focused predominantly on venom neutralisation rather than on promoting tissue repair.

Historically, adult stem cells have been positioned as regenerative agents through their differentiation capacity; however, it is now well established that their therapeutic benefit is predominantly mediated through paracrine signalling [19, 32, 33]. UCMSCs offer a particularly attractive source of such secreted molecules due to their scalability, availability and non-invasive isolation compared to other MSC sources. In this study, we provide the first evidence that conditioned medium (CM) from UCMSCs promotes the regeneration of skeletal muscle following damage induced by *Bitis arietans* (Puff adder) venom (BaV). We demonstrate that UCMSC CM appears to act by reprogramming the early regenerative environment rather than accelerating initial myofibre formation per se. In vitro, UCMSC CM was confirmed to target human muscle progenitor cells through uptake of extracellular vesicles. The proliferation of myoblasts was increased, without altering migration speed, indicating that the secretome promotes expansion of the myoblast pool. Furthermore, we demonstrate at the intracellular level that UCMSC CM increases lysosome and mitochondria mass in AB1190 cells. In the context of skeletal muscle, this could be interpreted as UCMSC-CM promoting the recycling of damaged molecules, potentially providing substrates to generate energy needed for cellular functions like mitosis [34]. Lastly, the inhibition of myoblast fusion suggests the maintenance of skeletal muscle precursors in a proliferative, metabolically active state.

Injury to skeletal muscle triggers a substantial local and systemic inflammatory response to orchestrate the clearance of necrotic fibres and activate the regenerative process, and

unresolved or excessive inflammation is a well-established driver of impaired regeneration and fibrosis. We demonstrated an ability for UCMSC CM to modulate the inflammatory environment through the master transcriptional regulator NF-κB, indicating a direct suppressive effect on innate immune cell activation and a pathway central to the transcriptional induction of pro-inflammatory cytokines and fibrotic remodelling when chronically active [35-38]. Importantly, with this suppression being partial rather than complete, it suggests that UCMSC CM recalibrates inflammatory signalling rather than abolishing it, maintaining the components of inflammation required for effective regeneration while limiting those that drive chronic damage and fibrosis.

Due to the multimodal capabilities of stem cell-secreted factors, we investigated whether possible effects of UCMSC CM are limited to enhancing regeneration, or if they can also work through the dampening of degenerative enzymes within venom directly. The biochemical profiling showed selective impacts of UCMSC CM on three classes of enzymes that are present in venom and implicated as major mediators of tissue damage [13, 15, 39-42]. The combination of a reduction in metalloproteinase activity at lower venom concentrations and the observed potentiation of serine protease activity introduces a complex interaction and suggests UCMSC CM does not function as a simple venom neutralising agent. These findings represent an important area for further investigation, particularly in defining whether it reflects direct enzymatic modulation, substrate-level effects, or indirect interactions mediated by CM components.

Our in vivo envenomation model showed, in agreement with previous studies, that BaV caused substantial damage to skeletal muscle with regeneration remaining incomplete by two weeks post-injury [27]. However, the degree of regeneration was increased with UCMSC CM

555 treatment as judged by the size of regenerated fibres, restoration of dystrophin localisation
556 [43] and the degree of fibrosis, which was underpinned by the decrease in the fibro-
557 adipogenic precursor marker PDGFRα. Despite the improvement in regeneration following
558 UCMSC CM treatment, there were still some signs of damage in muscles injured by BaV.
559 Skeletal muscle harbours an astonishing ability to regenerate, a process underpinned by an
560 orderly, temporally related series of events involving the activities of numerous cell types
561 capable of resolving in 2-3 weeks [44-47]. Persistent damage, as observed in chronic
562 neuromuscular disease, can result in disruption to this regenerative process, resulting in
563 impaired muscle fibre formation and fat and fibrotic tissue replacement [48-51]. In the case
564 of snake venom-induced muscle damage, we and others have postulated that the tissue also
565 undergoes continual damage since the injurious molecules are long-acting, in particular the
566 SVMPs [42, 52].

567 We suggest that the UCMSC CM is partly able to counteract the consequences of disrupted
568 skeletal muscle regeneration following the introduction of BaV. Although UCMSC CM
569 treatment failed to accelerate regeneration in the early period following BaV envenomation,
570 by 2 weeks post-injury the regenerated myofibres from the UCMSC CM-treated mice were
571 almost twice the size of than the vehicle-treated mice. This temporal pattern is consistent with
572 the in vitro finding that UCMSC CM expands the myoblast pool before differentiation. We
573 suggest that expansion of the myoblast population and their gradual transition into
574 differentiation would not necessarily produce larger fibres at the earliest regenerative
575 timepoint but would be expected to yield larger fibres once fusion and maturation proceeded,
576 thus offering a possible mechanistic explanation for the enlarged muscle fibres. UCMSC CM
577 treatment also restored dystrophin membrane circularity of regenerated myofibres,
578 statistically indistinguishable from healthy muscle. Together, these data indicate that UCMSC

CM's benefit in vivo is not confined to promoting large fibres alone but extends to structural maturity and membrane integrity of the regenerated tissue.

Next, we show that UCMSC CM limited the progression of fibrosis as measured by the control of fibro-adipogenic precursors (FAPs). These cells have pleiotropic properties; while being key to promoting regeneration through the activation of satellite cells, they can also lead to the formation of muscle fibrosis and fat [37, 53, 54]. Reciprocal signalling from developing muscle fibres promotes FAP proliferation [55], which in turn is limited by infiltrating pro-inflammatory macrophages secreting TNFα to induce FAP apoptosis. As the response resolves and macrophages shift toward an anti-inflammatory, pro-remodelling phenotype, the surviving FAPs begin to differentiate into myofibroblasts that ultimately lead to fibrotic deposits [48, 56]. Critically, this program depends on the inflammatory phase being self-limiting; the early TNFα burst must resolve on schedule for FAPs to be appropriately removed rather than persist.

We suggest the molecules in UCMSC CM either act directly on the FAPs to promote their apoptosis, or indirectly via dampening signals from other cells that would otherwise lead to the expansion and differentiation of this population. Given the anti-inflammatory property of UCMSC CM, specifically the NF-κB pathway, we hypothesise that the partial rather than complete NF-κB suppression, as seen with UCMSC CM in vitro, may be sufficient to temper the excessive, chronic inflammatory drive that sustains FAP persistence and fibrotic differentiation, while preserving sufficient early TNFα/NF-κB activity to support debris clearance and FAP apoptosis. Thus, an environment required for improved regeneration is created.

Lastly, we showed that UCMSC CM also reduced early intramuscular haemorrhage. Reduced fibrinogen accumulation at early time points suggests attenuation of vascular disruption

602 and/or enhancement of local haemostatic processes. We offer that this effect could plausibly
603 be explained by a combination of reduced metalloproteinase-mediated degradation of
604 vascular structures and a potential enhancement of local clotting pathways, as indicated by
605 potentiation of thrombin-like SVSP activity. Furthermore, we hypothesise that UCMSC CM
606 could act by supporting endothelial integrity and vascular stabilisation. While these
607 mechanisms remain to be directly validated, they point toward a multimodal effect on the
608 vascular component of muscle injury, which is a critical but often underappreciated
609 determinant of regenerative outcome.

610 Despite these benefits, UCMSC CM did not fully restore muscle architecture within the 15-day
611 window studied, and regenerated fibres in both injured groups remained smaller than healthy
612 tissue. BaV is a complex mixture of proteinaceous and non-proteinaceous molecules. Beyond
613 the three enzymes assessed in this study, snake venoms have a large and largely
614 uncharacterized repertoire of additional polypeptide species [57, 58] which UCMSC CM may
615 or may not interact with. We found that whilst lacking its own serine protease activity, UCMSC
616 CM potentiated the activity of the endogenous enzyme present in BaV. One intriguing
617 possibility, and an unresolved concern, is that while UCMSC CM has molecules that support
618 muscle regeneration, it could also have others that may attenuate this process.

619 From a translational perspective, the most significant implication of this work is the functional
620 separation between venom neutralisation and tissue regeneration. Current management of
621 snake envenomation centres on antivenom and, increasingly, the proposed use of adjunctive
622 small-molecule enzyme inhibitors such as varespladib and marimastat, both aimed at
623 neutralising venom components before they inflict further damage [39, 59, 60]. The real-world
624 duration between envenomation by *B. arietans* to the point when a treatment can be

administered needs to be considered. With an average of 5 hours for a patient to reach a hospital in the region of West Africa where *B. arietans* is present, it is likely that PLA2-mediated action, with a half-life of approximately 60 minutes [61], has induced extensive muscle fibre destruction and its remaining activity is minimal [46]. Hence in terms of treatment, therapies based on blocking venom PLA_2 activity such as varespladib [42] may often be ineffective. Several potent inhibitors of the long-lived SVMPs are currently being developed for the treatment of snake bites, including marimastat [42, 62]. We suggest their use needs careful deployment as while it may seem tempting to inhibit the activity of this class of enzyme in venom, it should be noted that normal muscle regeneration relies on remodelling of the ECM by endogenous MMPs. Therefore, robust inhibition of MMPs may hinder both venom molecules as well as muscle regeneration.

Finally, the halting of ongoing tissue destruction only addresses the injurious half of the clinical problem. Antivenoms and enzyme inhibitors primarily neutralise venom toxins and reduce further damage; they are not regenerative therapies that directly rebuild muscle, and their indirect benefit on muscle regeneration is impacted by the speed of administration [63]. Clinically, patients who survive envenomation, whether treated early or late, still face a prolonged and uncertain recovery of limb function, and fibrotic replacement of muscle is a recognised driver of long-term morbidity, chronic weakness, and disability in snakebite survivors. Our data suggest that UCMSC CM may complement antivenom and enzyme inhibitors by targeting muscle regeneration and fibrosis rather than neutralising venom enzymes. By treating alongside these strategies, a combination treatment could therefore address both the repair mechanisms as well as the ongoing toxin-mediated injuries. Such a combination strategy would not be constrained by the same narrow treatment-timing window that limits inhibitor efficacy alone, as UCMSC CM's regenerative and anti-fibrotic actions are

directed at tissue already committed to repair and so may retain therapeutic relevance even when the acute enzymatic injury phase has passed.

Conclusion

We show that UCMSC CM acts on multiple, complementary fronts to improve skeletal muscle regeneration following *B. arietans* venom-induced injury. In vitro, UCMSC CM is taken up by myoblasts and drives their expansion into a proliferative, metabolically active population while dampening excessive TNFα/NF-κB-driven inflammatory signalling. In vivo, these cellular and inflammatory effects translate into larger, more structurally mature, regenerated myofibres, reduced fibrosis accompanied by normalised fibro-adipogenic progenitor dynamics and reduced early intramuscular haemorrhage. Critically, these regenerative and anti-fibrotic actions address a therapeutic gap left open by current envenomation management.

List of abbreviations

BaV - *Bitis arietans* venom

CM - Conditioned media

CNF - Centrally nucleated fibres

eMHC - Embryonic myosin heavy chain

EV - Extracellular vesicle

FAP - Fibroadipogenic precursor

LPS - Lipopolysaccharide

NF-κB - Nuclear factor kappa-light-chain-enhancer of activated B cells

PLA_2 - Phospholipase A_2

SVMP - Snake venom metalloproteinase

SVSP - Snake venom serine protease

TA - *Tibialis anterior*

TGF-β - Transforming growth factor-beta

TNFα - Tumour necrosis factor alpha

UCMSC - Umbilical cord mesenchymal stem cell

Declarations

Ethics approval and consent to participate

Human umbilical cord-derived mesenchymal stem cells (UCMSCs) were purchased from RoosterBio®. The supplier confirmed that the source tissue was obtained with informed donor consent permitting research and further manufacturing use. Tissue was collected from donors in the USA per AATB, AABB, and FDA Regulations and tested using FDA approved methods.

Informed written consent was obtained from all human blood donors (or their legal representatives) prior to their participation in the study, including consent for the storage and use of tissue samples for research purposes. The collection and use of human blood for the project titled “Effects of Stem Cell Secretomes on Inflammation” was approved by the School of Biological Sciences’ Research Ethics Committee at the University of Reading, under the project approval code SBS22-23 41 on 25-Jan-2023.

All animal procedures were conducted in accordance with the Animals (Scientific Procedures) Act 1986 (ASPA) and the EU Directive 2010/63/EU, under UK Home Office project license

(project title: “Optimising skeletal muscle structure and function to withstand the challenges of damage and ageing”, licence number: PP8746932, approved on 06 September 2022) and personal licenses held by named individuals, at the University of Reading (establishment license: XF75DBBCB). The study was approved by the University of Reading's Animal Welfare and Ethics Review Board (AWERB) prior to commencement. Reporting follows the ARRIVE 2.0 guidelines.

Consent for publication

Not applicable

Availability of data and materials

All data generated or analysed during this study has been uploaded to Zenodo online repository under a reserved DOI: 10.5281/zenodo.23317307.

Competing Interests

AP, DF, RM & KP are current or past employees of the project funder, Micregen Ltd.

Funding

The work was funded by Micregen Limited.

Authors’ contributions

AP conceptualised and designed all experiments, generated in vitro myoblast and whole blood data, PIL-h who conducted in vivo work, sectioned and processed muscle samples, analysed and interpreted data, and wrote the manuscript. DF collected and analysed myoblast migration and enzyme assay data, PIL-h supporting in vivo work, captured and processed muscle images. MA generated in vitro myoblast Operetta imagery data and created protocols

and software for muscle histological analysis, and collected and analysed eMHC, CNF and dystrophin data. JW generated data for enzyme assays. AA generated and analysed NF-κB report cell data. DW conceptualised, created and provided NF-κB reporter cell, performed data analysis and interpretation. SV provided BaV material and resources for enzyme assays. RM conceptualised study design, PIL-h supporting in vivo work, analysed and interpreted data, reviewed and revised manuscript and had final approval of manuscript. KP conceptualised study design, interpreted data, wrote the manuscript and had final approval of the manuscript.

Acknowledgements

The authors thank the staff of the University of Reading Biological Resources Unit for animal husbandry and welfare support, and the blood donor volunteers who participated under ethics approval SBS22-23 41. We thank the extended R&D team at Micregen Ltd, and members of Patel, Vaiyapuri and Widera labs at the University of Reading for additional support towards this project.

Perplexity AI was used to assist with refining the grammar, sentence structure and flow of the Introduction and Discussion sections. All conceptualisation, data analysis, and critical interpretations were performed independently by the human authors, who verify and assume full responsibility for the final text.

References

1. Frontera, W.R. and J. Ochala, *Skeletal muscle: a brief review of structure and function.* Calcif Tissue Int, 2015. **96**(3): p. 183-95.

2. Collins, C.A., et al., *Stem cell function, self-renewal, and behavioral heterogeneity of cells from the adult muscle satellite cell niche.* Cell, 2005. **122**(2): p. 289-301.
3. Lee, J.E., et al., *Regulatory Landscapes of Muscle Satellite Cells: From Mechanism to Application.* Int J Stem Cells, 2025. **18**(3): p. 237-253.
4. Mann, C.J., et al., *Aberrant repair and fibrosis development in skeletal muscle.* Skelet Muscle, 2011. **1**(1): p. 21.
5. Gutiérrez, J.M., et al., *Why is Skeletal Muscle Regeneration Impaired after Myonecrosis Induced by Viperid Snake Venoms?* Toxins (Basel), 2018. **10**(5).
6. Bhaumik, S., et al., *How and why snakebite became a global health priority: a policy analysis.* BMJ Glob Health, 2023. **8**(8).
7. Allen, S. and J.K. Chakma, *Toward achieving the WHO 2030 target in the mitigation of snakebite envenoming: the fundamental challenges in addressing the unmet needs.* Trop Med Health, 2025. **53**(1): p. 74.
8. Chippaux, J.P., *Snakebite envenomation turns again into a neglected tropical disease!* J Venom Anim Toxins Incl Trop Dis, 2017. **23**: p. 38.
9. Pintor, A.F.V., et al., *Addressing the global snakebite crisis with geo-spatial analyses - Recent advances and future direction.* Toxicon X, 2021. **11**: p. 100076.
10. Kasturiratne, A., D.G. Lalloo, and H. Janaka de Silva, *Chronic health effects and cost of snakebite.* Toxicon X, 2021. **9-10**: p. 100074.
11. Vishnu, K.S., S. Dineshbabu, and T. Kadhiravan, *Functional Disability at 3 Months in Patients with Residual Limb Swelling after Snakebite Envenoming.* Am J Trop Med Hyg, 2024. **111**(5): p. 1142-1144.
12. Ralph, R., et al., *Managing snakebite.* Bmj, 2022. **376**: p. e057926.

13. Itang, S.I., et al., *Comparative venomics and preclinical evaluation of antivenoms against Nigeria's "big three" snakes: Naja nigricollis, Bitis arietans, and Echis ocellatus.* Toxicon, 2026. **281**: p. 109194.
14. Tianyi, F.L., et al., *Clinical features of puff adder envenoming: case series of Bitis arietans snakebites in Kenya and a scoping review of the literature.* PLoS Negl Trop Dis, 2025. **19**(2): p. e0012845.
15. Dawson, C.A., et al., *Intraspecific venom variation in the medically important puff adder (Bitis arietans): Comparative venom gland transcriptomics, in vitro venom activity and immunological recognition by antivenom.* PLoS Negl Trop Dis, 2024. **18**(10): p. e0012570.
16. Biehl, J.K. and B. Russell, *Introduction to stem cell therapy.* J Cardiovasc Nurs, 2009. **24**(2): p. 98-103; quiz 104-5.
17. Sandonà, M., et al., *Mesenchymal Stromal Cells and Their Secretome: New Therapeutic Perspectives for Skeletal Muscle Regeneration.* Front Bioeng Biotechnol, 2021. **9**: p. 652970.
18. Squecco, R., et al., *Bone Marrow-Mesenchymal Stromal Cell Secretome as Conditioned Medium Relieves Experimental Skeletal Muscle Damage Induced by Ex Vivo Eccentric Contraction.* Int J Mol Sci, 2021. **22**(7).
19. Gnecchi, M., et al., *Paracrine Mechanisms of Mesenchymal Stem Cells in Tissue Repair.* Methods Mol Biol, 2016. **1416**: p. 123-46.
20. Aziziyan, F., et al., *Mesenchymal stem cell-derived extracellular vesicles in musculoskeletal regeneration: mechanisms, applications, and future prospects.* Stem Cell Res Ther, 2026. **17**(1): p. 66.

21. Song, Y., et al., *Human mesenchymal stem cells derived from umbilical cord and bone marrow exert immunomodulatory effects in different mechanisms.* World J Stem Cells, 2020. **12**(9): p. 1032-1049.
22. Wang, W., et al., *Autophagy of umbilical cord mesenchymal stem cells induced by rapamycin conduces to pro-angiogenic function of the conditioned medium.* Biochem Biophys Rep, 2023. **36**: p. 101583.
23. Batsali, A.K., et al., *Mesenchymal stem cells derived from Wharton's Jelly of the umbilical cord: biological properties and emerging clinical applications.* Curr Stem Cell Res Ther, 2013. **8**(2): p. 144-55.
24. Piccinini, F., A. Kiss, and P. Horvath, *CellTracker (not only) for dummies.* Bioinformatics, 2016. **32**(6): p. 955-957.
25. Noë, S., et al., *The Myotube Analyzer: how to assess myogenic features in muscle stem cells.* Skeletal Muscle, 2022. **12**(1): p. 12.
26. Asadpour, A., et al., *Neural Crest-Derived Stem Cell Secretomes and Extracellular Vesicles Disrupt Glioblastoma through Dual-Pathway Inflammatory Rebalancing.* Stem Cell Rev Rep, 2026. **22**(5): p. 2528-2548.
27. Adeyemi, S.O., et al., *Compromised Regeneration, Damage to Blood Vessels and the Endomysium Underpin Permanent Muscle Damage Induced by Puff Adder (Bitis arietans) Venom.* Toxins (Basel), 2025. **17**(10).
28. Mitchell, R., et al., *Secretome of adipose-derived mesenchymal stem cells promotes skeletal muscle regeneration through synergistic action of extracellular vesicle cargo and soluble proteins.* Stem Cell Res Ther, 2019. **10**(1): p. 116.
29. Pachitariu, M., M. Rariden, and C. Stringer, *Cellpose-SAM: superhuman generalization for cellular segmentation.* bioRxiv, 2025: p. 2025.04.28.651001.

30. Waisman, A., et al., *Automatic and unbiased segmentation and quantification of myofibers in skeletal muscle.* Scientific Reports, 2021. **11**(1): p. 11793.
31. Godoi, K.S., et al., *Anti-Metalloproteases: Production and Characterization of Polyclonal IgG Anti-F2 Fraction Antibodies Purified from the Venom of the Snake Bitis arietans.* Toxins (Basel), 2023. **15**(4).
32. Gnecchi, M., et al., *Evidence supporting paracrine hypothesis for Akt-modified mesenchymal stem cell-mediated cardiac protection and functional improvement.* Faseb j, 2006. **20**(6): p. 661-9.
33. Smolinská, V., M. Boháč, and Ľ. Danišovič, *Current status of the applications of conditioned media derived from mesenchymal stem cells for regenerative medicine.* Physiol Res, 2023. **72**(S3): p. S233-s245.
34. Audano, M., A. Schneider, and N. Mitro, *Mitochondria, lysosomes, and dysfunction: their meaning in neurodegeneration.* J Neurochem, 2018. **147**(3): p. 291-309.
35. Vallabhapurapu, S. and M. Karin, *Regulation and function of NF-kappaB transcription factors in the immune system.* Annu Rev Immunol, 2009. **27**: p. 693-733.
36. Bakkar, N. and D.C. Guttridge, *NF-kappaB signaling: a tale of two pathways in skeletal myogenesis.* Physiol Rev, 2010. **90**(2): p. 495-511.
37. Joe, A.W., et al., *Muscle injury activates resident fibro/adipogenic progenitors that facilitate myogenesis.* Nat Cell Biol, 2010. **12**(2): p. 153-63.
38. Ren, N., et al., *The nuclear factor kappa B signaling pathway is a master regulator of renal fibrosis.* Front Pharmacol, 2023. **14**: p. 1335094.
39. Clare, R.H., et al., *Repurposed small molecule toxin inhibitors neutralise a diversity of venoms from the Neotropical viperid snake genus Bothrops*. 2026, eLife Sciences Publications, Ltd.

40. Hardy, D., et al., *Comparative Study of Injury Models for Studying Muscle Regeneration in Mice.* PLoS One, 2016. **11**(1): p. e0147198.
41. Rao, S., et al., *The Role of Snake Venom Proteins in Inducing Inflammation Post-Envenomation: An Overview on Mechanistic Insights and Treatment Strategies.* Toxins (Basel), 2024. **16**(12).
42. Williams, H.F., et al., *Mechanisms underpinning the permanent muscle damage induced by snake venom metalloprotease.* PLoS Negl Trop Dis, 2019. **13**(1): p. e0007041.
43. Dowling, P., D. Swandulla, and K. Ohlendieck, *Cellular pathogenesis of Duchenne muscular dystrophy: progressive myofibre degeneration, chronic inflammation, reactive myofibrosis and satellite cell dysfunction.* Eur J Transl Myol, 2023. **33**(4).
44. Forcina, L., M. Cosentino, and A. Musarò, *Mechanisms Regulating Muscle Regeneration: Insights into the Interrelated and Time-Dependent Phases of Tissue Healing.* Cells, 2020. **9**(5).
45. Musarò, A., *Muscle Homeostasis and Regeneration: From Molecular Mechanisms to Therapeutic Opportunities.* Cells, 2020. **9**(9).
46. Dixon, R.W. and J.B. Harris, *Myotoxic activity of the toxic phospholipase, notexin, from the venom of the Australian tiger snake.* J Neuropathol Exp Neurol, 1996. **55**(12): p. 1230-7.
47. Meyer, G.A., *Evidence of induced muscle regeneration persists for years in the mouse.* Muscle Nerve, 2018. **58**(6): p. 858-862.
48. Yin, K., et al., *FAPs orchestrate homeostasis of muscle physiology and pathophysiology.* Faseb j, 2024. **38**(24): p. e70234.

850 49. Villalobos, E., P. Mehra, and J. Diaz-Manera, *From fibro/adipogenic progenitors to*
851 *adipocytes: Understanding adipogenesis in muscle degeneration for disease*
852 *modulation.* J Physiol, 2025. **603**(19): p. 5273-5297.
853 50. Molina, T., P. Fabre, and N.A. Dumont, *Fibro-adipogenic progenitors in skeletal muscle*
854 *homeostasis, regeneration and diseases.* Open Biol, 2021. **11**(12): p. 210110.
855 51. Theret, M., F.M.V. Rossi, and O. Contreras, *Evolving Roles of Muscle-Resident Fibro-*
856 *Adipogenic Progenitors in Health, Regeneration, Neuromuscular Disorders, and Aging.*
857 Frontiers in Physiology, 2021. **Volume 12 - 2021**.
858 52. Saravia-Otten, P., et al., *Homogenates of skeletal muscle injected with snake venom*
859 *inhibit myogenic differentiation in cell culture.* Muscle Nerve, 2013. **47**(2): p. 202-12.
860 53. Contreras, O., F.M.V. Rossi, and M. Theret, *Origins, potency, and heterogeneity of*
861 *skeletal muscle fibro-adipogenic progenitors-time for new definitions.* Skelet Muscle,
862 2021. **11**(1): p. 16.
863 54. Mozzetta, C., et al., *Fibroadipogenic progenitors mediate the ability of HDAC inhibitors*
864 *to promote regeneration in dystrophic muscles of young, but not old Mdx mice.* EMBO
865 Mol Med, 2013. **5**(4): p. 626-39.
866 55. Kang, X., et al., *Interleukin-15 facilitates muscle regeneration through modulation of*
867 *fibro/adipogenic progenitors.* Cell Commun Signal, 2018. **16**(1): p. 42.
868 56. Nawaz, A., et al., *Depletion of CD206(+) M2-like macrophages induces fibro-adipogenic*
869 *progenitors activation and muscle regeneration.* Nat Commun, 2022. **13**(1): p. 7058.
870 57. Godoi, K.S., et al., *Conserved Enzymatic Peptides in Bitis arietans Venom Revealed by*
871 *Comparative Proteomics: Implications for Cross-Reactive Antibody Targeting.* Int J Mol
872 Sci, 2026. **27**(3).

58. Adeyi, A.O., et al., *Preliminary Insights into Geographic Variation in Venom Profiles and Functional Activities of Nigerian Snakes, Bitis arietans and Naja nigricollis.* Toxins (Basel), 2026. **18**(5).
59. Lewin, M.R., et al., *Varespladib in the Treatment of Snakebite Envenoming: Development History and Preclinical Evidence Supporting Advancement to Clinical Trials in Patients Bitten by Venomous Snakes.* Toxins (Basel), 2022. **14**(11).
60. Layfield, H.J., et al., *Repurposing Cancer Drugs Batimastat and Marimastat to Inhibit the Activity of a Group I Metalloprotease from the Venom of the Western Diamondback Rattlesnake, Crotalus atrox.* Toxins (Basel), 2020. **12**(5).
61. Sanhajariya, S., S.B. Duffull, and G.K. Isbister, *Pharmacokinetics of Snake Venom.* Toxins (Basel), 2018. **10**(2).
62. !!! INVALID CITATION !!! [64].
63. Xiao, H., et al., *Inactivation of Venom PLA_2 Alleviates Myonecrosis and Facilitates Muscle Regeneration in Envenomed Mice: A Time Course Observation.* Molecules, 2018. **23**(8).

Figure Legends

Figure 1. In vitro study of UCMSC CM mechanisms of action on immortalized human myoblasts and inflammation.

(A) Representative images of UCMSC PKH-stained EV (green) uptake in AB1190 (red) at 24 hours (scale bar 50 µM). (B) Intensity of PKH-EV staining per cell at 24 hours (n=6). (C) Effect of UCMSC CM on AB1190 proliferation (n=8) and (D) on AB1190 migration (n=25). (E) Effect of UCMSC CM on lysosome mass and (F) mitochondria mass in AB1190 at 24 hours (n=4). (G) Representative images of AB1190 differentiation by fusion indicated by pan-myosin (green)

positive myotubes (scale bar 500 µM). (H) Effect of UCMSC CM on AB1190 differentiation assessed with a fusion index – ratio of nuclei per myotube vs total nuclei (n=4). (I) Effect of dose-wise UCMSC CM treatment on whole human blood stimulated with LPS, assessed by ELISA for TNFα release. Treatment concentrations given as "x" concentration of 10% v/v (n=4). (J) Effect of UCMSC CM on NF-κB signalling pathway activation using U251-NF-κB-luciferease report cell stimulated with TNFα (n=4 baseline and vehicle controls and n=3 UCMSC CM treatment). Statistical significance was considered when $p<0.05$.

Figure 2. Assessment of UCMSC CM on BaV enzymatic activity.

(A) Enzyme kinetics for the effect of UCMSC CM on metalloproteinase activity, and (B) serine protease activity over 90 minutes at different BaV concentrations. (C) Enzyme kinetics for the effect of UCMSC CM on phospholipase A_2 activity over 120 minutes at different BaV concentrations. Statistical significance was considered when $p<0.05$.

Figure 3. Assessment of UCMSC CM on myofibre regeneration post BaV injury.

(A) Representative images from immunohistochemistry for embryonic myosin heavy chain (eMHC) positive regenerating myofibres (red) and laminin in the ECM (green) (scale bar 500 µM). (B) Representative images from immunohistochemistry for dystrophin in undamaged, day 5 post-injury, and day 15 post-injury (scale bar 500 µM). (C) Effect of UCMSC CM on muscle regeneration at day 5 post BaV injury, by assessing the cross-sectional area of eMHC-positive myofibres (n=6 vehicle and n=7 UCMSC CM). (D) Effect of UCMSC CM on muscle regeneration at day 15 post BaV injury, by assessing the cross-sectional area of centrally located myofibres (n=4 undamaged, n=8 vehicle, n=7 UCMSC CM). (E) Effect of UCMSC CM on dystrophin expression at day 15 post BaV injury (n=4 undamaged, n=8 vehicle, n=7 UCMSC CM). Statistical significance was considered when $p<0.05$.

Figure 4. Assessment of UCMSC CM effect on fibrosis post BaV injury.

(A) Representative images of H&E histology of TA cross-sections from undamaged, day 5 post-injury, and day 15 post-injury (scale bar 200 μM). Red arrows = regenerating fibres, white arrows = infiltrated non-myogenic cells, green = fibrotic lesions. (B) Representative images of picrosirius red histology of TA cross-sections from undamaged, day 5 post-injury, and day 15 post-injury (scale bar 500 μM). White arrows = infiltrated non-myogenic cells; green = fibrotic lesions. (B) Representative images from immunohistochemistry for platelet-derived growth factor receptor-alpha (PDGFRα) positive fibro-adipogenic (FAPs) cells (scale bar 500 μM). (C) Effect of UCMSC CM on fibrosis at day 5 and day 15 post BaV injury (n=5 undamaged, n=6 day 5 vehicle, n=7 day 5 UCMSC CM and day 15 UCMSC CM, n=8 day 15 vehicle). (D) Effect of UCMSC CM on FAPs at day 5 and day 15 post BaV injury, by assessing the level of PDGFRα (n=5 undamaged, n=6 day 5 vehicle and day 15 UCMSC CM, n=7 day 5 UCMSC CM, n=8 day 15 vehicle). Statistical significance was considered when $p<0.05$.

Figure 5. Assessment of UCMSC CM on haemorrhage in skeletal muscle post BaV injury.

(A) Representative images from immunohistochemistry for fibrinogen in undamaged, day 5 post-injury, and day 15 post-injury (scale bar 500 μM). (B) Effect of UCMSC CM on the BaV-induced haemorrhage within TA muscle by assessing the presence of fibrinogen at day 5 and day 15 post BaV injury (n=5 undamaged, n=6 day 5 vehicle and day 5 UCMSC CM, n=7 day 15 UCMSC CM, n=8 day 15 vehicle). Statistical significance was considered as $p<0.05$.

Figure 1

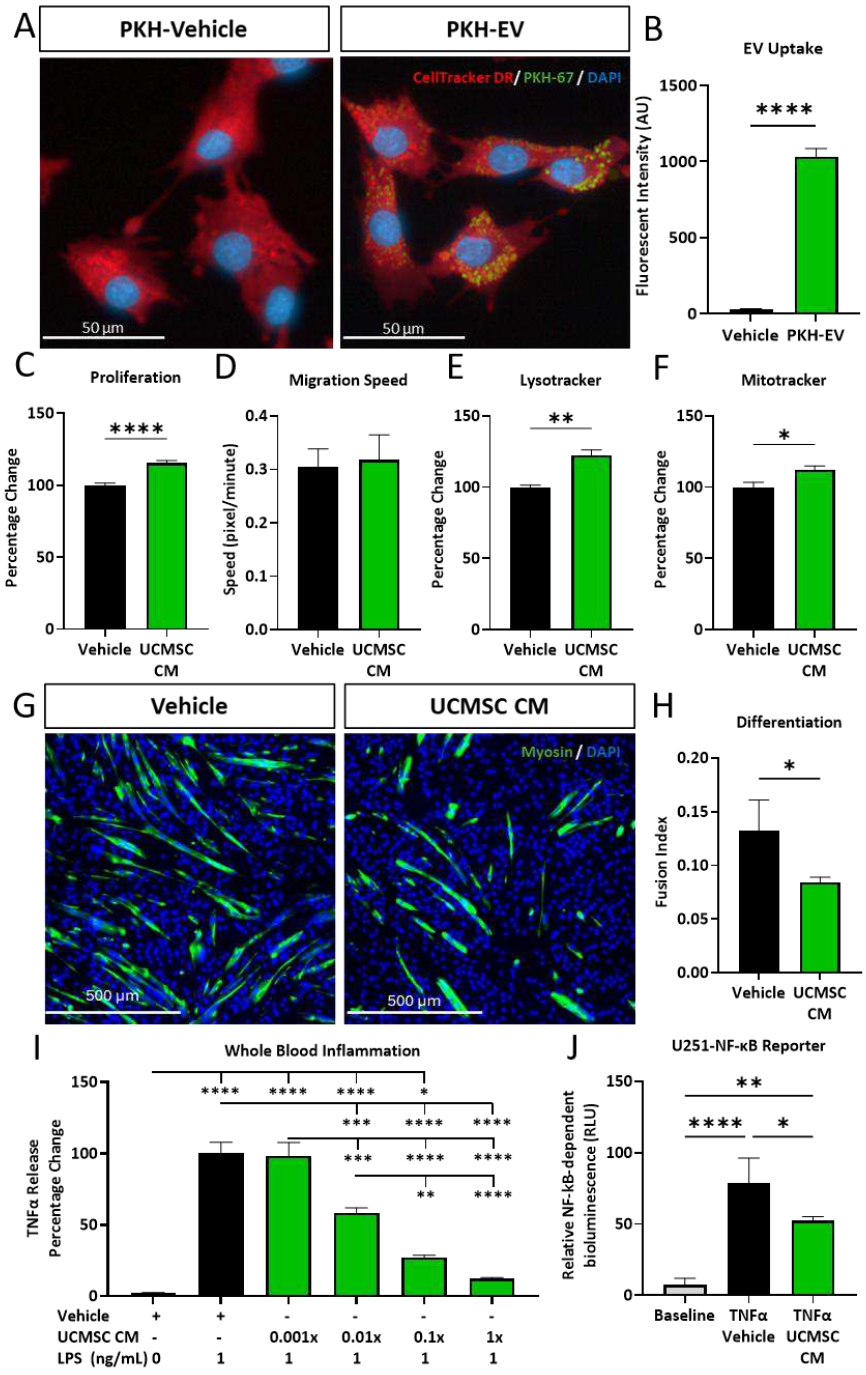

A
PKH-Vehicle
PKH-EV
CellTracker DR / PKH-67 / DAPI
50 µm
50 µm
B
EV Uptake
Fluorescent Intensity (AU)
****
Vehicle
PKH-EV
C
Proliferation
Percentage Change
****
Vehicle
UCMSC CM
D
Migration Speed
Speed (pixel/minute)
Vehicle
UCMSC CM
E
Lysotracker
Percentage Change
**
Vehicle
UCMSC CM
F
Mitotracker
Percentage Change
*
Vehicle
UCMSC CM
G
Vehicle
UCMSC CM
Myosin / DAPI
500 µm
500 µm
H
Differentiation
Fusion Index
*
Vehicle
UCMSC CM
I
Whole Blood Inflammation
TNFα Release Percentage Change
Vehicle
UCMSC CM
LPS (ng/mL)
0
1
0.001x
0.01x
0.1x
1x
J
U251-NF-κB Reporter
Relative NF-kB-dependent bioluminescence (RLU)
**
****
*
Baseline
TNFα Vehicle
TNFα UCMSC CM

Figure 2

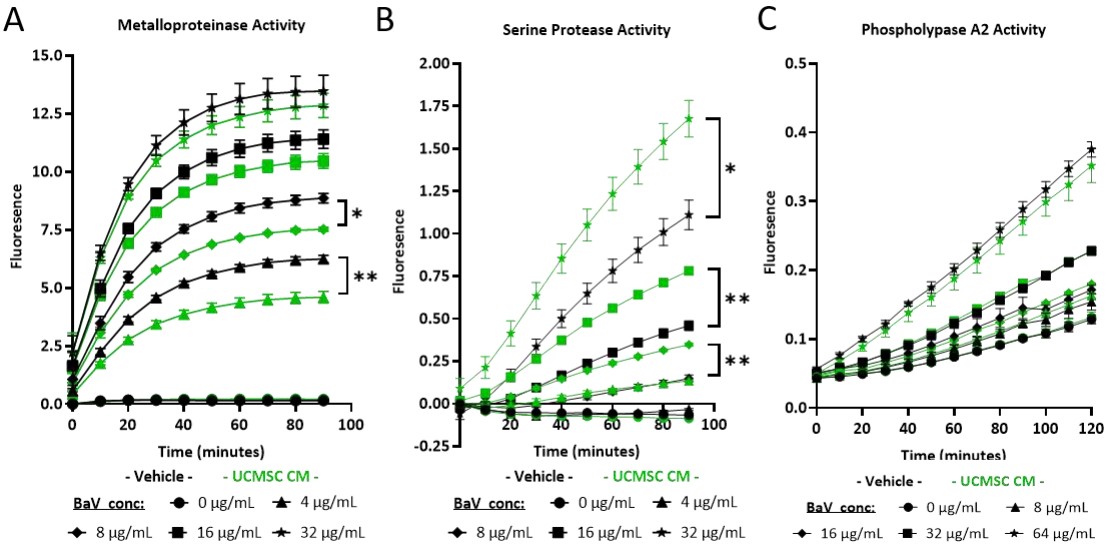

A
Metalloproteinase Activity
Fluoresence
Time (minutes)
- Vehicle -
- UCMSC CM -
BaV conc:
0 µg/mL
4 µg/mL
8 µg/mL
16 µg/mL
32 µg/mL
B
Serine Protease Activity
Fluoresence
Time (minutes)
- Vehicle -
- UCMSC CM -
BaV conc:
0 µg/mL
4 µg/mL
8 µg/mL
16 µg/mL
32 µg/mL
C
Phospholypase A2 Activity
Fluoresence
Time (minutes)
- Vehicle -
- UCMSC CM -
BaV conc:
0 µg/mL
8 µg/mL
16 µg/mL
32 µg/mL
64 µg/mL

Figure 3

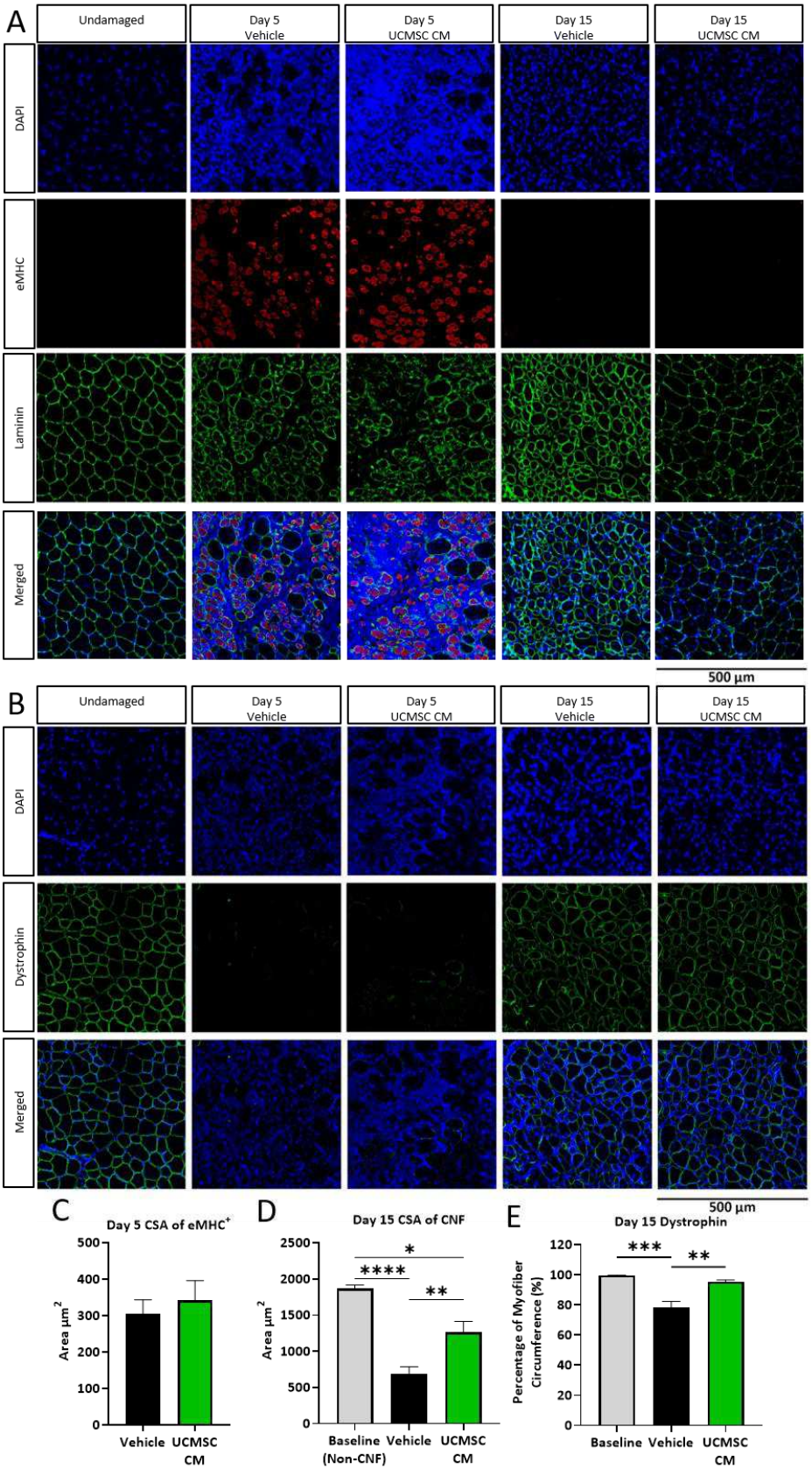

A
Undamaged
Day 5 Vehicle
Day 5 UCMSC CM
Day 15 Vehicle
Day 15 UCMSC CM
DAPI
eMHC
Laminin
Merged
500 µm
B
Undamaged
Day 5 Vehicle
Day 5 UCMSC CM
Day 15 Vehicle
Day 15 UCMSC CM
DAPI
Dystrophin
Merged
500 µm
C
Day 5 CSA of eMHC+
Area µm2
Vehicle
UCMSC CM
D
Day 15 CSA of CNF
Area µm2
Baseline (Non-CNF)
Vehicle
UCMSC CM
E
Day 15 Dystrophin
Percentage of Myofiber Circumference (%)
Baseline
Vehicle
UCMSC CM

Figure 4

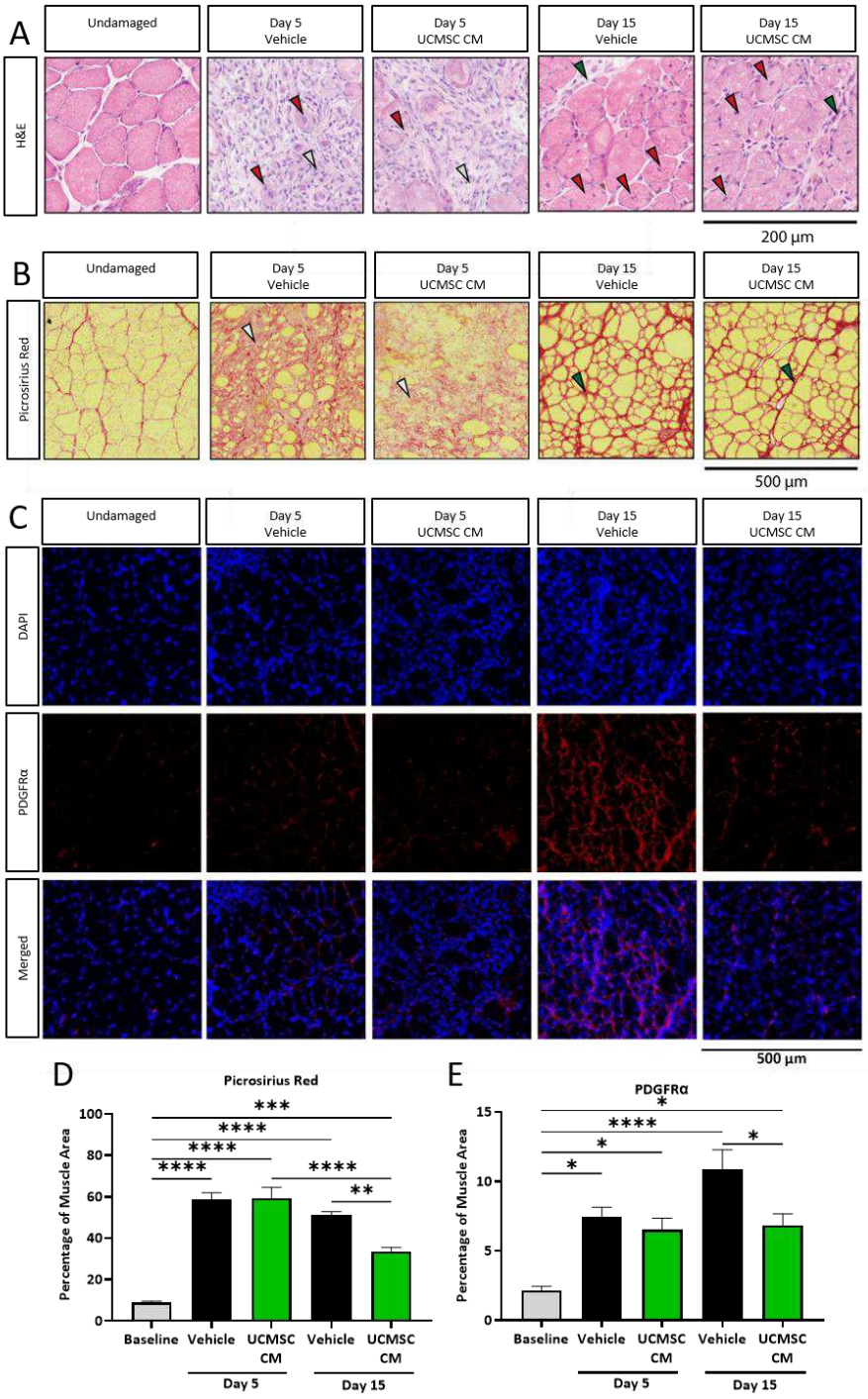
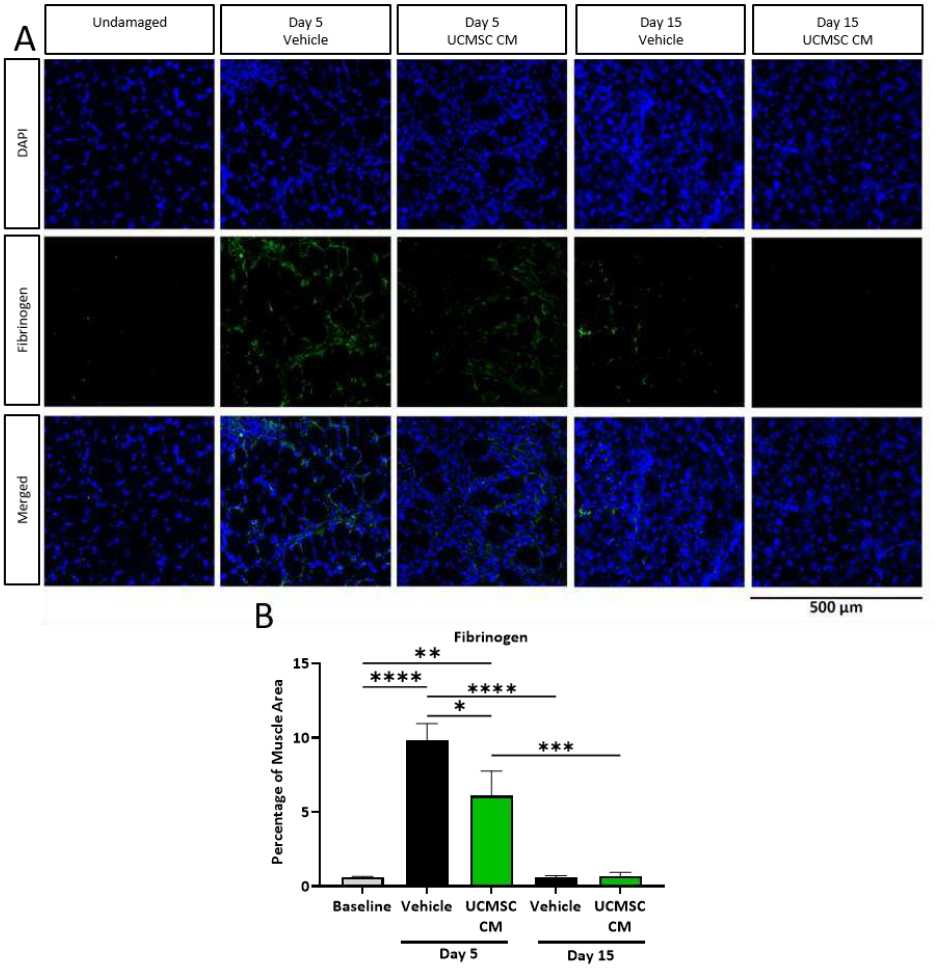

A
Undamaged
Day 5 Vehicle
Day 5 UCMSC CM
Day 15 Vehicle
Day 15 UCMSC CM
H&E
200 µm
B
Undamaged
Day 5 Vehicle
Day 5 UCMSC CM
Day 15 Vehicle
Day 15 UCMSC CM
Picrosirius Red
500 µm
C
Undamaged
Day 5 Vehicle
Day 5 UCMSC CM
Day 15 Vehicle
Day 15 UCMSC CM
DAPI
PDGFRα
Merged
500 µm
D
Picrosirius Red
Percentage of Muscle Area
Baseline
Vehicle
UCMSC CM
Vehicle
UCMSC CM
Day 5
Day 15
E
PDGFRα
Percentage of Muscle Area
Baseline
Vehicle
UCMSC CM
Vehicle
UCMSC CM
Day 5
Day 15

Figure 5


A
Undamaged
Day 5 Vehicle
Day 5 UCMSC CM
Day 15 Vehicle
Day 15 UCMSC CM
DAPI
Fibrinogen
Merged
500 µm
B
Fibrinogen
Percentage of Muscle Area
15
10
5
0
**
****
****
*
***
Baseline
Vehicle
UCMSC CM
Vehicle
UCMSC CM
Day 5
Day 15